Structure
Article

Molecular Basis of SMC ATPase Activation: Role of Internal Structural Changes of the Regulatory Subcomplex ScpAB

Katsuhiko Kamada,[1,*] Makoto Miyata,[2] and Tatsuya Hirano[1,*]
[1]Chromosome Dynamics Laboratory, RIKEN Advanced Science Institute, 2-1 Hirosawa, Wako, Saitama 351-0198, Japan
[2]Department of Biology, Graduate School of Science, Osaka City University, Sumiyoshi-ku, Osaka 558-8585, Japan
*Correspondence: kamadak@riken.jp (K.K.), hiranot@riken.jp (T.H.)
http://dx.doi.org/10.1016/j.str.2013.02.016

SUMMARY

In many bacteria, a homodimer of structural-maintenance-of-chromosomes proteins associates with two regulatory subunits (known as ScpA and ScpB), assembling a protein complex that plays a crucial role in chromosome organization and segregation. It remains poorly understood, however, how this complex might work at the mechanistic level. Here, we report crystal structures of the ScpAB core complex that display a highly unusual structure in which the central segment of ScpA winds around an asymmetrically oriented ScpB dimer. The two C-terminal domains of the ScpB dimer primarily interact with different regions of ScpA with different affinities. Moreover, flexible interdomain regions of ScpB contribute to a dynamic folding process of the ScpAB subcomplex. Together with other genetic and biochemical assays, we provide evidence that internal structural changes of the ScpAB subcomplex are tightly coupled with activation of the structural-maintenance-of-chromosomes ATPase.

INTRODUCTION

Structural-maintenance-of-chromosomes (SMC) protein complexes are some of the most fundamental molecular machineries that regulate large-scale chromosome organization and functions from bacteria to humans (Losada and Hirano, 2005; Nasmyth and Haering, 2005). In eukaryotes, heteromeric SMC dimers constitute the core of the cohesin and condensin complexes that play central roles in sister-chromatid cohesion and chromosome condensation, respectively (Hirano, 2012; Onn et al., 2008; Peters et al., 2008). In bacteria, a homomeric SMC dimer functions as the core of a condensin-like complex (Graumann and Knust, 2009). Both heteromeric and homomeric SMC dimers display a highly characteristic V-shaped architecture that has two ATP-binding-cassette-type "head" domains at its distal ends (Anderson et al., 2002; Melby et al., 1998). ATP binding and hydrolysis control engagement and disengagement of the SMC head domains, and it is believed that such a catalytic cycle regulates dynamic interaction of the SMC dimer with DNA.

In the Gram-positive bacterium *Bacillus subtilis*, the SMC protein, together with its regulatory subunits, ScpA and ScpB, participates in global organization and segregation of chromosomes (Britton et al., 1998; Jensen and Shapiro, 1999; Mascarenhas et al., 2002; Moriya et al., 1998; Soppa et al., 2002). Like SMC, ScpA and ScpB are widely conserved among prokaryotes (Mascarenhas et al., 2002; Volkov et al., 2003). Null mutations in these three genes cause a similar set of defective phenotypes: chromosome organization and segregation are grossly compromised, leading to the formation of anucleate cells at high frequencies. ScpA and ScpB are colocalized with SMC to form discrete foci, and these three proteins are positioned interdependently in vivo (Lindow et al., 2002; Volkov et al., 2003). In fact, ScpA interacts with the SMC head domain and ScpB, supporting the assembly of a ternary complex in vitro, while ScpB does not apparently bind to SMC. The exact subunit stoichiometry of the two factors in the complex remains controversial (Fuentes-Perez et al., 2012; Hirano and Hirano, 2004; Mascarenhas et al., 2005). Crystal structures of ScpB from *Chlorobium tepidum* and *Mycobacterium tuberculosis* demonstrate that ScpB forms a stable dimer through its N-terminal winged-helix domain (Kim et al., 2006, 2008). No structural information is currently available for ScpA or the ScpAB complex, and the mechanism of activation of SMC ATPase by ScpA and ScpB, is not fully understood.

In a subfamily of γ-proteobacteria including *Escherichia coli*, a distinct complex known as MukBEF is believed to function as a structural and functional homolog of SMC-ScpAB (Yamazoe et al., 1999), although the corresponding subunits (i.e., MukB/SMC, MukE/ScpB, and MukF/ScpA) share very little similarity to each other at the primary structure level. For instance, MukF is much larger than ScpA and has the ability to form a stable dimeric core (Fennell-Fezzie et al., 2005). MukB compacts single DNA molecules in a highly cooperative manner in vitro (Cui et al., 2008). The MukEF subcomplex stimulates MukB's ATPase activity (Woo et al., 2009) but restricts DNA reshaping mediated by MukB (Petrushenko et al., 2006). Biochemical and crystallographic studies have revealed that ATP-dependent engagement of MukB head domains disrupts a MukB-MukF interaction (Woo et al., 2009). It was proposed that the ATP-hydrolysis energy is utilized for subunit rearrangement, leading to the oligomerization of MukB through a rigid structural bridge composed of the MukEF subcomplex. It remains unknown whether a similar mechanism might also operate in the action of SMC-ScpAB.

In the current study, we report the crystal structure of a functional subcomplex of the *Geobacillus stearothermophilus* ScpAB. The ScpAB core complex displays an unprecedented structure in which a central segment of ScpA winds around an asymmetrically oriented ScpB dimer. A combination of biochemical and genetic data provide evidence that this structure represents a latent form of ScpAB, which conceals the central segment of ScpA required for stimulation of the SMC ATPase activity. Our results strongly suggest that dynamic internal structural changes of the ScpAB subcomplex actively regulate SMC ATPase activity, and they offer broad implications for our understanding of the action of bacterial and eukaryotic SMC protein complexes.

RESULTS AND DISCUSSION

Structure Determination of the ScpAB Core Complex

Two SMC regulatory subunits, ScpA and ScpB, from *G. stearothermophilus* were coexpressed and purified as a complex. As judged by gel filtration and SDS-PAGE, the recombinant behaves as a single protein complex, with an apparent stoichiometry of 2:4. Limited proteolysis and mass spectrometry analyses demonstrated that ScpA in the complex form has a domain boundary that separates its C-terminal domain from the rest of the part (Figure S1A available online). On the basis of the information obtained, we redesigned expression constructs, and found that ScpA lacks its C-terminal region (1–174) and that ScpB trimmed from both flexible ends (12–191) formed an ~61 kDa complex with 1:2 stoichiometry in good homogeneity (Figures S2A and S2B). We interpreted these results as follows. The C-terminal domain of ScpA would bind to the SMC head domain when it was available, as had been demonstrated for other kleisin subunits (Haering et al., 2004; Woo et al., 2009), and as will be shown later in this study. In the initially purified fraction of full-length ScpAB, the ScpA C-terminal domains weakly associated with each other to form an apparent dimer unit, because its exposed hydrophobic surface needed to be hidden under the aqueous solutions where the intrinsic binding partner (i.e., the SMC head domain) was absent. In the current study, the second, truncated version of the complex (henceforth referred to as the ScpAB core) was crystallized, and its structure was determined by the single-anomalous-dispersion method, and was refined to a resolution of 2.6 Å (Table 1).

Table 1. Data Collection and Refinement Statistics for ScpAB Complexes

	ScpAB Core Native	ScpAB Core MeHgCl Derivative	ScpB NTD-ScpA Peptide
Data Collection			
Space group	$P2_1$	$P2_1$	$C2$
Cell Dimensions			
a, *b*, *c* (Å)	90.86, 127.42, 97.22	90.91, 127.59, 97.10	107.82, 88.92, 60.68
α, β, γ (°)	90, 113.84, 90	90, 113.69, 90	90, 94.31, 90
Peak			
Wavelength	1.00000	1.00556	1.00000
Resolution (Å)	50.0–2.6	50.0–2.65	50.0–2.4
R_{sym}[a]	6.3 (66.9)	5.6 (40.8)	5.1 (11.6)
$I/\sigma I$	19.8 (1.6)	18.6 (1.5)	17.2 (8.4)
Completeness (%)	98.5 (89.5)	97.1 (79.6)	99.4 (89.8)
Redundancy	3.9 (3.6)	1.9 (1.7)	3.8 (3.6)
Figure of Merit[b]			
Acentric/Centric		0.297/0.143	
Total		0.274	
Refinement			
Resolution (Å)	30.7-2.6		46-2.4
No. of reflections	61,951		23,058
R_{work}/R_{free}[c]	0.225/0.266		0.236/0.285
No. of Atoms			
Protein	7,505		2,860
Solvent	43		101
B-Factors (Å^2)			
Protein	67.60		35.38
Solvent	40.36		35.42
Rmsd[d]			
Bond lengths (Å)	0.009		0.009
Bond angles (°)	1.181		1.296

Values in parentheses are for the highest-resolution shell.
[a] $R_{sym} = \Sigma|I - \langle I\rangle|/\Sigma I$, where I is the observed intensity and $\langle I\rangle$ is the average intensity obtained from multiple observations of symmetry-related reflections.
[b] Figure of merit = $\sum P(\alpha)e^{i\alpha}/\sum P(\alpha)$, where α is the phase and $P(\alpha)$ is the phase probability distribution.
[c] Free R factor was calculated with 5% of randomly selected data omitted from the structure refinement.
[d] Root-mean-square deviation (Rmsd) bond lengths and Rmsd bond angles are the respective Rmsds from ideal values.

ScpA Winds around an Asymmetrically Oriented ScpB Dimer

The ScpAB core structure is composed of four winged-helix domains (wHDs) from the ScpB homodimer with a single polypeptide of ScpA (Figures 1A and 1B). Electrostatic calculations of the complex showed that the molecular surface is largely acidic (Figures S3A–S3C). Each ScpB protomer consists of two tandem-aligned wHDs that are connected by an interdomain (ID) region (Figure 1B). The N-terminal wHD (NTD) is responsible for dimerization of ScpB within the core complex, as has been described previously in the structures of ScpB homodimer free of ScpA (Kim et al., 2006, 2008). Intriguingly, however, unlike in the ScpA-free ScpB homodimer, the two C-terminal wHDs (CTDs) of ScpB are asymmetrically oriented within the core complex (Figure S3D). In our ScpAB core structure, the CTD of the anterior ScpB ($ScpB_{an}$) binds to helix H5 of ScpA, whereas the CTD of the posterior ScpB ($ScpB_{po}$) binds to helix H7 of ScpA. Moreover, the central segment of ScpA is located underneath the NTD dimer and winds around the ID region of $ScpB_{po}$ (Figure 1A). This unexpected folding of the ScpAB core complex is achieved by a series of local interactions between residues of ScpA and ScpB, which in turn stabilize the overall structure of the heterotrimeric complex. In addition, the two ID regions in the ScpB homodimer adopt different conformations to maintain

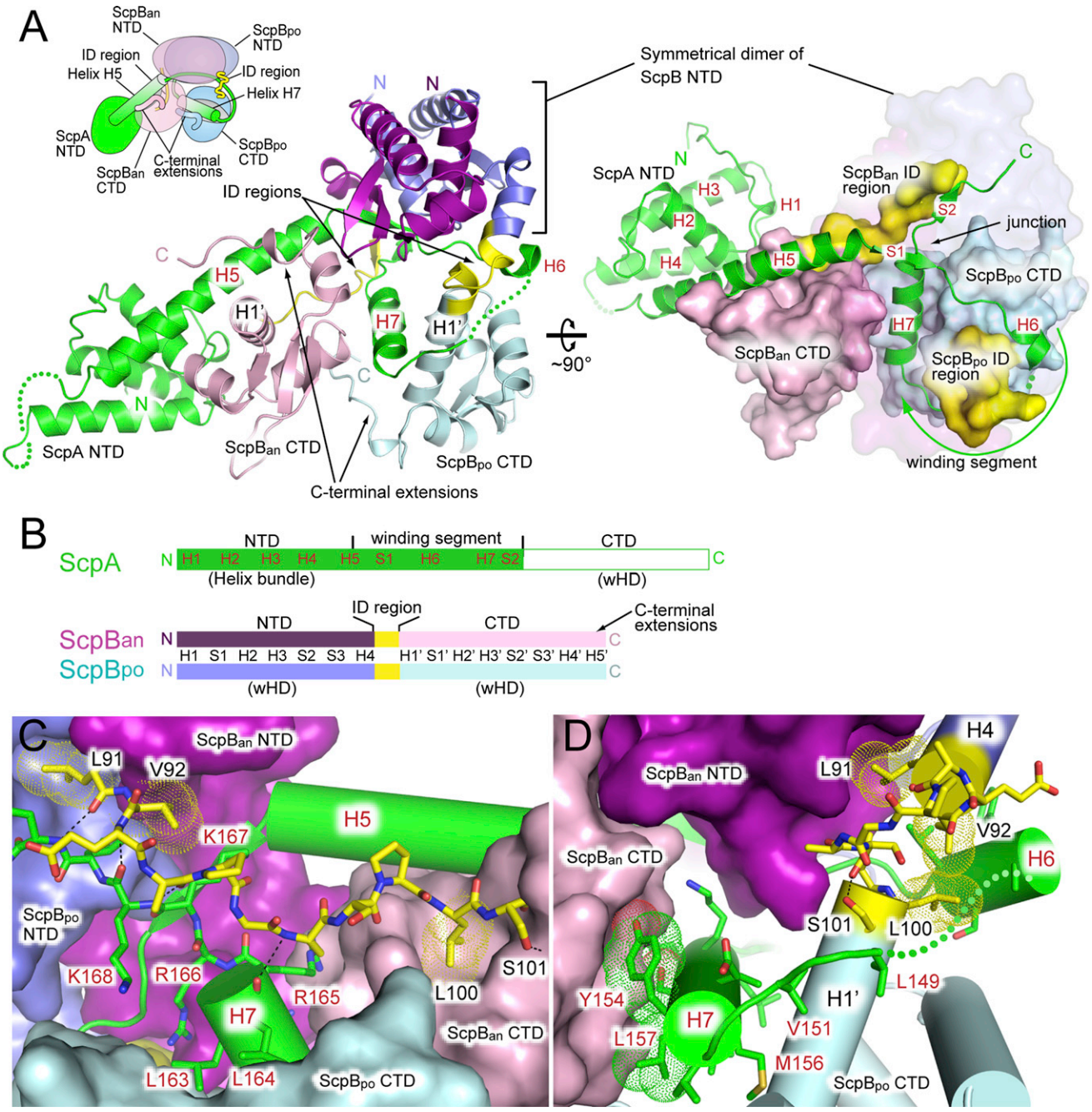

Figure 1. Structure of the ScpAB Core Complex

(A) Overall structure of the ScpAB core complex with schematic drawings. Shown at left is a ribbon drawing and its schematic representation of the ScpA monomer bound to the ScpB homodimer viewed perpendicular to the 2-fold axis of the symmetrical ScpB N-terminal dimer. The N- and C-termini of the subunits and principal secondary-structure elements are labeled. Shown at right is the junction region of the ScpA winding segment viewed from the top with surface representation of ScpB, except that the N-terminal dimer is transparent.

(B) Domain architecture of ScpA and ScpB. ScpA is comprised of the N-terminal helix-bundled domain (NTD), a central winding segment, and the C-terminal winged-helix domain (CTD). The ScpA CTD is shown here as a blank bar, because it is not included in the crystal structure. ScpB is composed of the N-terminal winged-helix domain (magenta and slate), an interdomain (ID) region (yellow) and the winged-helix C-terminal domain (light pink and cyan).

(C) Details of the $ScpB_{an}$ ID region. The extended peptide forms a short antiparallel β sheet with the peptide following from the ScpA helix H7.

(D) Details of the $ScpB_{po}$ ID region. A structural constraint imposed by the winding segment makes the ID region fold compactly by partial helix extensions from both H4 and H1′ helices.

See also Figures S1–S4 and Table S1.

the characteristic form of the complex (Figures 1C and 1D). Thus, the ScpB dimer contributes to the folding of ScpA in a highly intricate manner, so that the resulting trimeric subcomplex forms a compact architecture.

Although it had previously been predicted that the ScpA NTD is folded into a winged helix (Fennell-Fezzie et al., 2005), we noticed that the domain in our structure contains only four short helices. Alignment by the Dail server (Holm and Rosenström, 2010) demonstrated that spatial orientation of the secondary structural elements within the ScpA NTD is dissimilar to that of a typical wHD, and that the ScpA NTD rather resembles a four-helix-bundle domain. In fact, *E. coli* MukF has a four-helix-bundle domain in the corresponding position, apart from its N-terminal wHD that is responsible for dimerization (Figures S4A and S4B). These considerations, together with the homogenous properties of the ScpAB core complex, suggest that the ScpA NTD is unlikely to be responsible for its own dimerization. Helix H5, which stems from the ScpA NTD, primarily contributes to its interaction with the $ScpB_{an}$ CTD (Figure 1A). The following short segments of ScpA, strand S1 and helix H6, contact underneath the dimeric ScpB NTD, and are curved down along the edge of the ID region of $ScpB_{po}$. After a short missing region with low electron density, the next helix of ScpA, H7, is sandwiched between the two ScpB CTDs (Figure 1D), and the subsequent strand, S2, is located under and across the peptide. In this junction point, the downstream region of ScpA does not make significant contact with strand S1 but forms a short antiparallel β sheet with the ID region of $ScpB_{an}$ (Figure 1C).

Dual Recognition Scheme of the ScpB CTD for ScpA Binding

Binding areas between ScpA and ScpB dimers are extensive (the total buried surface area is ~3,900 $Å^2$), and more than half of the residues in the ScpA winding segment participate in its intermolecular contacts with ScpB (Figure S1A). In particular, binding of ScpA helices H5 and H7 to the ScpB CTDs occupies about half of the areas (~1,170 $Å^2$ and ~750 $Å^2$, respectively). ScpA helix H5 is laid almost perpendicular to $ScpB_{an}$ helix H1' (Figure 2A), and a similar orientation is preserved between ScpA helix H7 and $ScpB_{po}$ helix H1' (Figure 2B). Moreover, bulky hydrophobic residues of ScpA, Leu119 in helix H5 and Met156 in helix H7, recognize the deepest dents of the $ScpB_{an}$ and $ScpB_{po}$ CTDs, respectively. It is very interesting to note, however, that the H5 and H7 helices of ScpA are oppositely oriented relative to the ScpB CTDs, so that surface residues of the two CTDs are organized to form suitable contacts for each ScpA helix. For example, the bulky residue Phe112 in ScpA helix H5 makes a close contact with Leu179 of $ScpB_{an}$ (Figure 2A). On the other hand, Leu160 and Leu164, located on the same surface of the ScpA H7 helix, are distant from Leu179 of $ScpB_{po}$ and instead make contact with Trp182 (Figure 2B), which is invisible in $ScpB_{an}$. In another case, Leu100 of $ScpB_{an}$ is engaged to form a hydrophobic surface with its neighboring residue, Leu105, to make a contact with the aliphatic portion of Lys120 of ScpA helix H5 (Figure 2A). In the $ScpB_{po}$ CTD, however, the corresponding Leu100 is flipped back in the opposite direction, and Leu149 and Val151 of ScpA compensate by filling the hollowed surface of the $ScpB_{po}$ CTD and stabilizing the L-shaped form of ScpA (Figure 2B). The conformational change of Leu100 is assisted by motion of the neighboring conserved residue Ser101, which alters its hydrogen-bond partners of main-chain atoms (Figures S3E and S3F). Interestingly, the two types of peptide trajectories to the ScpB CTD have been observed in two different crystal structures of ScpA-free ScpB homodimer (Figure S3E). Thus, it is most likely that Ser101 acts as a key determinant in facilitating the dual binding modes of the ScpB CTD. The C-terminal extension of the ScpB CTDs can be traced clearly in the ScpAB core structure (Figure 1A), although they were not visible in the ScpA-free ScpB structures reported previously (Figure S3E). This disorder-to-order transition seems to be essential for formation of the complex.

To further assess the differential contributions of the two ScpB CTDs to their binding to ScpA, we applied isothermal titration calorimetry (ITC). The dissociation constant (Kd) for ScpB(12–191)/ScpA(1–174), the pair of materials used for crystallization, was estimated to be ~56 nM (Figure 2C), and the stoichiometry of ScpB/ScpA was close to 2. Interestingly, whereas the ScpB CTD(98–217) bound to ScpA(1–143) with a 1:1 stoichiometry, the Kd for them was close to the value found with the ScpAB complex (~51 nM; Figure 2D). In striking contrast, the binding of ScpB CTD to a synthetic peptide, ScpA(147–166), was much weaker than those mentioned above (Kd = ~2.2 μM) (Figure 2E). Another titration analysis using the ScpB CTD and ScpA(1–174) presented a reasonable simultaneous fitting for the two sites (Kd = ~32 nM and ~0.29 μM) (Figure 2F). These results suggest that the tight binding of the $ScpB_{an}$ CTD to ScpA helix H5 (and the ScpA NTD) makes a primary contribution to the stoichiometric formation of the complex. The contribution of the weaker binding of $ScpB_{po}$ to ScpA helix H7 is secondary, implying that there exists a structural hierarchy in the folding process to make the unusual architecture of the ScpAB core complex.

A Variable ScpB ID Region Guides the Assembly of the ScpAB Complex

Part of the winding segment of ScpA (from strand S1 to helix H6) is housed by the symmetrical ScpB NTD dimer. Nonetheless, our ITC experiments failed to detect binding of the ScpB NTD (12–99) dimer to a synthetic ScpA peptide (125–142), suggesting that interaction between the two is rather weak. Then how might the dimerized ScpB NTDs contribute to holding the ScpA winding segment? To address this question, we attempted another crystallographic approach and obtained crystals of ScpB NTD (12–99) dimer with a synthetic ScpA peptide (125–142). The structure was solved by molecular replacement using the NTD dimer from the ScpAB core complex as a search model. The model was refined to a resolution of 2.4 Å with good stereochemistry (Table 1).

The structure of the ScpB NTD dimer in this crystal was essentially identical to that seen in the ScpAB core complex (Figure 3A). The synthetic ScpA peptide is also accommodated, with a fixed orientation, in a trench on the underside of the symmetric NTD dimer. We noticed, however, that the ID region of $ScpB_{an}$ in this structure displays a different conformation, forming a short stretch of an antiparallel β sheet with the N-terminal half of the ScpA peptide (Figure 3A). Pro95 in the ID region contributes to making local hydrophobic contacts with the bulky Phe130 residue of the ScpA peptide on the $ScpB_{an}$ NTD surface.

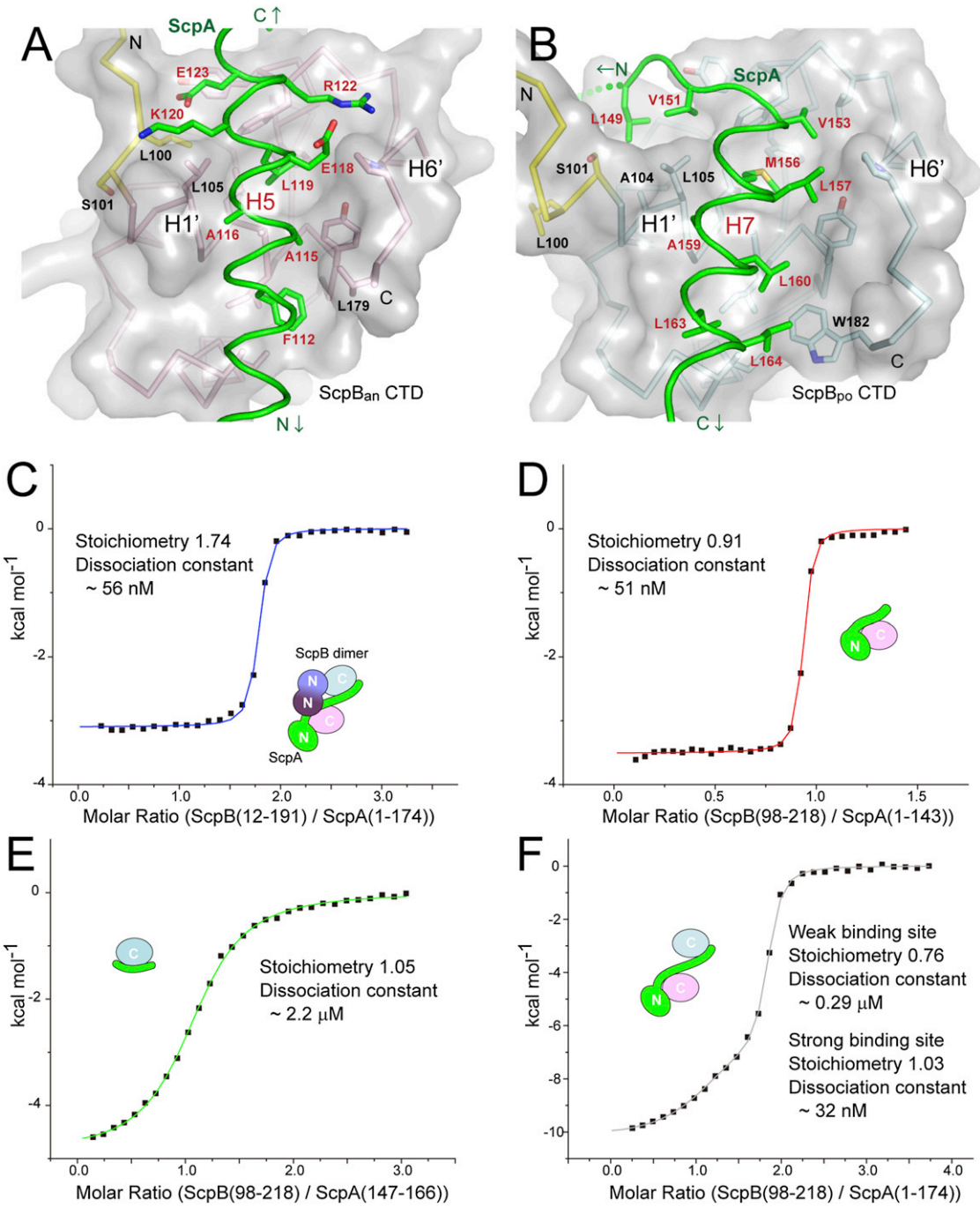

Figure 2. Molecular Properties of Two ScpB CTDs for ScpA Binding

(A and B) Close-up views of two amphipathic helices of ScpA, H5 (A) and H7 (B), bound to the hydrophobic concave surface of the ScpB CTD. Hydrophobic residues involved in these interfaces are shown along with the molecular surface of ScpB CTDs. Two key residues (Leu100 and Ser101) in the $ScpB_{po}$ ID region are also shown (see also Figure S3F).

(C–F) Isothermal titration calorimetry data for interactions between various constructs of ScpA and ScpB. The calorimetric titrations of 0.66 mM of ScpB(12–191) into 0.040 mM of ScpA(1–174) with $1.8 \times 10^7 \pm 2.1 \times 10^6$ M^{-1} of K_b (C), 0.73 mM of ScpB(98–217) into 0.050 mM of ScpA(1–143) with $2.0 \times 10^7 \pm 2.4 \times 10^6$ M^{-1} of K_b (D), 0.73 mM of ScpB(98–217) into 0.050 mM of ScpA(147–166) with $4.6 \times 10^5 \pm 2.1 \times 10^4$ M^{-1} of K_b (E), and 0.73 mM of ScpB(98–217) into 0.040 mM of ScpA(1–174) with $3.5 \times 10^6 \pm 3.3 \times 10^5$ M^{-1} and $3.1 \times 10^7 \pm 8.1 \times 10^6$ M^{-1} of K_b for two sites (F). The curves in the ITC panels are fit to a one-set-of-sites model, except for (F), which is fit to two sets of sites.

See also Figure S3 and Table S1.

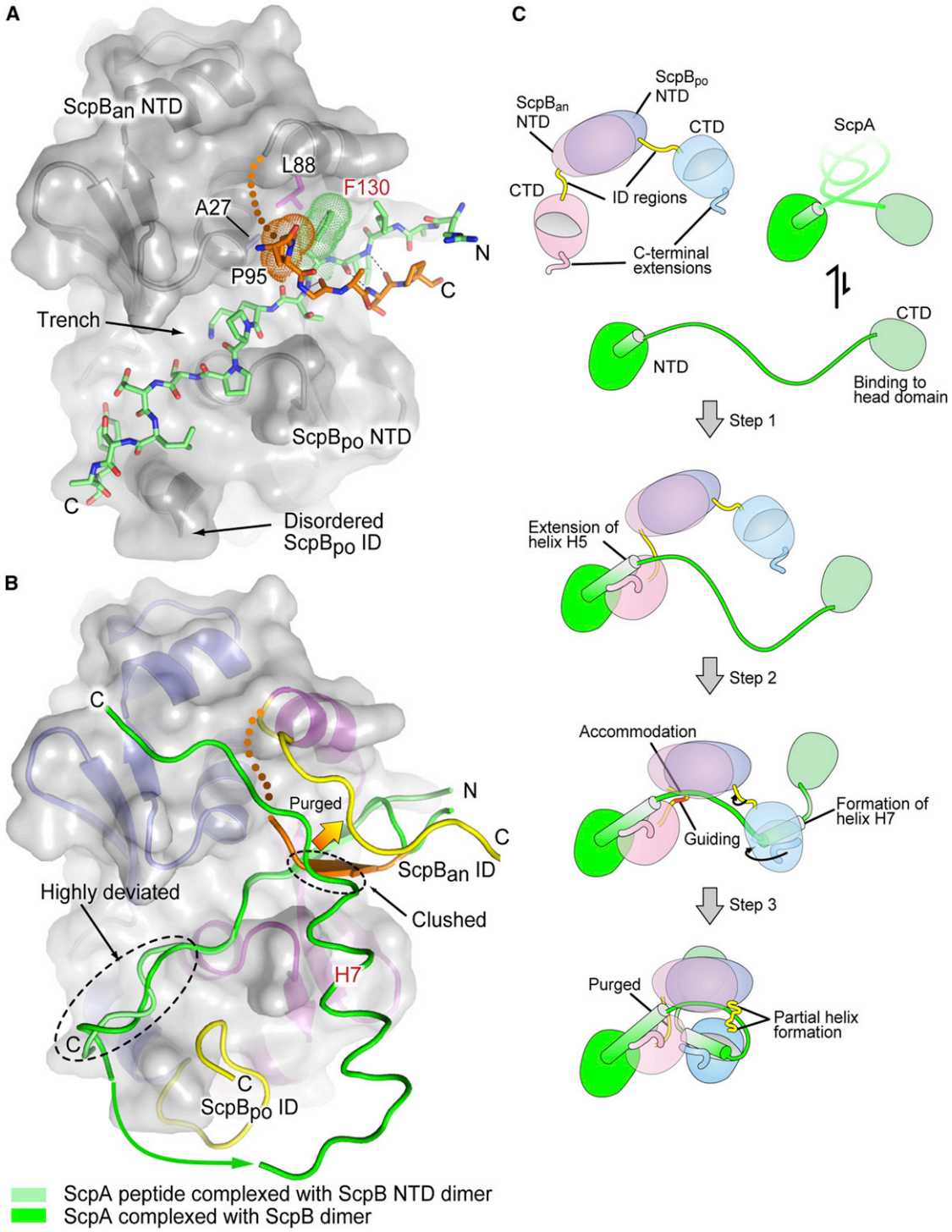

Figure 3. Structure of ScpB NTD Dimer with an ScpA Peptide and Folding Steps of the ScpAB Core Complex

(A) Detailed view of the ScpB NTD dimer (gray) complexed with the ScpA peptide (125–142; light green). The $ScpB_{an}$ ID region (from Ala94 to Pro99; orange) alters its conformation and captures the ScpA peptide.

(B) Exploded view of the junction point of ScpA with two complex structures superimposed using NTD dimer structures. The $ScpB_{an}$ ID region seen in the NTD dimer complex (orange) is spatially incompatible with a subsequent region from the end of helix H7 of the ScpAB complex.

(C) Schematic diagram of the predicted folding scheme of ScpAB. Binding of the $ScpB_{an}$ CTD to the ScpA NTD directs binding of the $ScpB_{po}$ CTD to ScpA helix H7. Helix H5 of ScpA would extend substantially when it interacts with the $ScpB_{an}$ CTD, while helix H7 would be induced to form upon binding to the $ScpB_{po}$ CTD. The ID region of $ScpB_{an}$ guides ScpA interaction underneath the NTD dimer, and then is purged aside to finalize the formation of the closed form of ScpAB.

Moreover, the next residue, Gly96, modulates the conformation of the rest of the ID region so that it runs alongside the ScpA peptide. Although this interacting region of the ScpA peptide is well ordered and follows the same trajectory observed in the ScpAB core complex, the following helix, H6, is highly deviated due to weak density (Figure 3B). The ID region of $ScpB_{an}$ recognizes the ScpA peptide, following helix H5. In contrast, the ID region of $ScpB_{po}$ is totally disordered in this structure (Figure 3B). It is suggested that the $ScpB_{an}$ ID region guides a smooth placement of the ScpA peptide underneath the ScpB NTD dimer after the $ScpB_{an}$ CTD recognizes ScpA helix H5.

Proposed Steps for ScpAB Subcomplex Formation

The current study provides structural insights into a series of steps that support the assembly and folding of the ScpAB complex. When monomeric ScpA is expressed as a recombinant polypeptide, it is highly sensitive to proteases, indicating that the bulk of ScpA is disordered and undergoes a disorder-to-order transition upon binding to ScpB. We suggest that binding of ScpA helix H5 to the $ScpB_{an}$ CTD represents the initial step of the whole assembly process, which is further reinforced by an induced-fit binding of the C-terminal extension of $ScpB_{an}$ (Figure 3C, step 1). The dimerized ScpB NTDs not only provide a platform for placing ScpA underneath them, but also ensure that the second CTD (i.e., the $ScpB_{po}$ CTD) is placed in close proximity to helix H7 (Figure 3C, step 2). At this step, the two ID regions in the ScpB dimer change their own conformations and work as adjusters to help fine-tune the global architecture of the ScpAB complex. The ID region of $ScpB_{an}$ plays a guiding role so that the region following ScpA helix H5 is eventually placed underneath the dimerized NTDs of ScpA (Figure 3A). Once the $ScpB_{po}$ CTD captures helix H7, it rotates around its own ID region (Figure 3C, step 3). Finally, helix H7 makes an additional contact with the $ScpB_{ap}$ CTD and is sealed by the C-terminal extension of $ScpB_{po}$. Notably, the electrostatic-potential surface surrounding the ScpA junction point is strongly negatively charged (Figure S3C), whereas the ScpA sequence following the H7 helix contains positively charged residues, suggesting that docking of the highly polarized surfaces could provide a major driving force to wind up the bound unit of ScpA H7-$ScpB_{po}$ CTD. We also infer that rotation of the bound unit induces partial helix formation in the $ScpB_{po}$ ID region (Figure 1A), which helps complete the folding of the ScpAB core complex. At the same time, the ID region of $ScpB_{an}$ finishes its role in introducing the ScpA peptide underneath the ScpB NTD dimer and is released upon completion of the folding process (Figures 3B and 3C, step 3).

Genetic Dissection of the ScpAB Subcomplex

To understand the role of individual domains in the regulatory subcomplex in vivo, we set up genetic analyses in *B. subtilis*. It had been shown previously that disruption of either *scpA* or *scpB* causes temperature-sensitive lethality in complex media, as had been demonstrated for *smc* (Soppa et al., 2002). Therefore, we first constructed strains in which an isopropyl-β-D-1-thiogalactopyranoside (IPTG)-inducible promoter controls the endogenous level of BsScpAB or BsScpB alone (Figures S5A and S5B). Then, mutant versions of BsScpA or BsScpB were exogenously expressed in these strains under the control of a xylose-responsive promoter and assessed for their viability under the condition where expression of the endogenous genes was reduced (−IPTG + xylose).

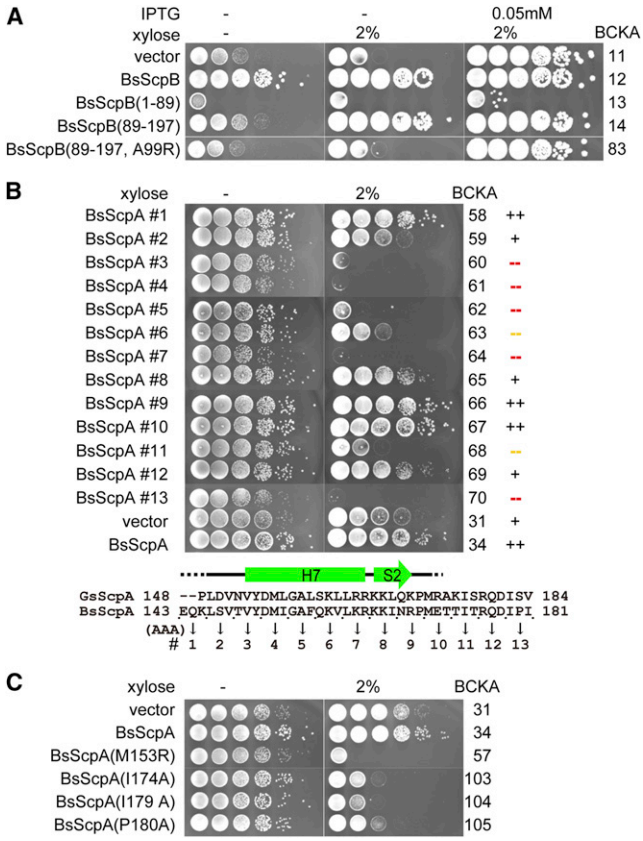

Figure 4. Dominant-Negative Effects of ScpA and ScpB Mutations In Vivo

(A) The viability of the BCKA4-based strains expressing functional domains of BsScpB. Serial (10-fold) dilutions of their cultures were spotted on agar plates containing the indicated concentrations of IPTG or xylose.

(B) The viability of the BCKA3-based strains expressing BsScpA with various 3-Ala mutations in its helix H7. The sequence of the mutated region of BsScpA is indicated at the bottom.

(C) The viability of the BCKA3-based strains expressing BsScpA with point mutations around its helix H7 region.

See Figures S5, S6, and Table S2.

When the endogenous level of BsScpB is reduced in the parental strain, cell growth is greatly impaired (Figure 4A, BCKA11). Expression of full-length BsScpB restored cell viability under this condition (BCKA12). To our surprise, expression of the BsScpB CTD also restored cell viability (BCKA14). Introduction of a mutation into the BsScpA-binding surface of BsScpB (A99R) abolished its ability to restore viability (BCKA83). Moreover, we found that expression of the BsScpB CTD alone was able to rescue even an *scpB* null mutant at 37°C (Figure S6). On the other hand, expression of the BsScpB NTD displayed a dominant-negative effect in both the presence and absence of IPTG (BCKA13), implying that NTDs might sequester functional BsScpA under these conditions. The most plausible interpretation for this phenotype is that the exogenously expressed NTD causes inactivation of endogenous BsScpB by heterodimer

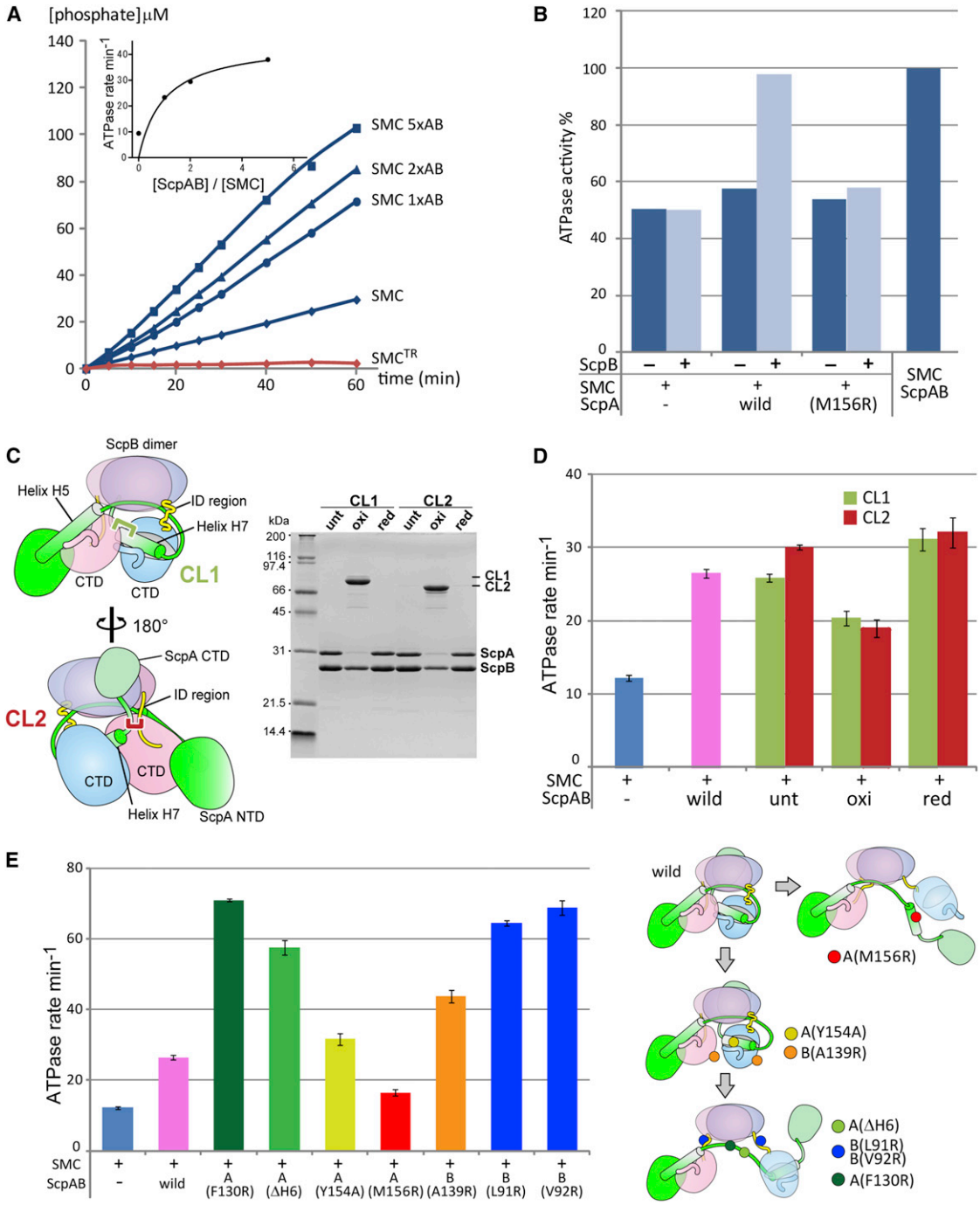

Figure 5. Effects of Intrasubcomplex Motion of ScpAB on SMC ATPase Activity

(A) Time course of ATP hydrolysis by full-length SMC (50 nM [blue]) in the absence (diamonds) and presence of ScpAB. ScpAB was added to SMC at 1-fold (circles), 2-fold (triangles), or 5-fold (squares) molar ratios. Also shown is ATP hydrolysis by the transition-state mutant, SMC^{TR} (red). The smooth curve of the hydrolysis rate in the inset is the best fits to the data using the Michaelis-Menten equation. The estimated V_{max} and K_m values were 45 min^{-1} and 0.97, respectively.

(B) Effects of adding individually purified regulatory subunits on SMC ATPase. ATPase activities of full-length SMC (50 nM), with ScpA (wild-type and M156R mutant) (50 nM) in the absence or presence of ScpB (100 nM), and with purified ScpAB complex (50 nM) were measured. The activities are plotted as percentages of a reference activity of SMC plus ScpAB.

(C) Schematic representations showing two disulfide-bridging sites used in crosslinking experiments (left). Shown at right are electrophoretic mobility shifts of double cysteine mutants. The two mutated ScpAB complexes (CL1 and CL2) were either untreated (unt), oxidized (oxi), or oxidized and then reduced (red) before being subjected to nonreducing SDS-PAGE. The crosslinked products are indicated by CL1 and CL2 on the right.

(legend continued on next page)

formation, which in turn reduces binding frequency of the BsScpB CTD for two sites of BsScpA. Thus, these observations substantiate the functional importance of the ScpB CTD in vivo.

We next asked whether the weak interaction between the ScpA helix H7 and $ScpB_{po}$ CTD might play a critical role in vivo. To this end, we used another parental strain in which the endogenous levels of both BsScpA and BsScpB were equally reduced (Figures S5A and S5B, BCKA3). Because the extent of reduction was modest and balanced, compared with the BsScpB-deficient strain (Figure 4A, BCKA12), cell viability was not severely affected in the absence of IPTG (Figure 4B, BCKA31). We then replaced three successive residues in or near helix H7 with alanines and expressed these mutant versions of BsScpA in the parental strain. Remarkably, it was found that expression of some of the BsScpA mutants displayed a strong dominant-negative effect (i.e., Figure 4B, BCKA60, 61, 62, 64, and 70). Furthermore, a single amino acid substitution of arginine for Met153 (corresponding to Met156 in GsScpA) was sufficient to suppress cell growth (Figure 4C, BCKA57). These results underscore the importance of hydrophobic residues in ScpA helix H7 that are involved in binding to the $ScpB_{po}$ CTD. Finally, similar observations were made when hydrophobic residues (Ile174, Ile179, and Pro180), located between the H7 helix and the CTD of ScpA, were replaced with alanine (Figure 4C, BCKA103–105), implying that this flexible region, missing in our crystal structure, also plays an important function.

Evidence that Dynamic Conformational Changes of ScpAB Modulate SMC ATPase

To investigate the role of ScpAB in regulating SMC ATPase activity, we expressed and purified full-length SMC and various functional domains of ScpA and/or ScpB (Figure S7A). The wild-type SMC possessed a basal activity of ATP hydrolysis (~11 ATP/min/mol), whereas its transition-state mutant (E1118Q) displayed virtually no activity (Figure 5A). Addition of purified ScpAB complex substantially increased the ATPase activity of SMC in a dose-dependent manner, although addition of ScpA or ScpB alone barely or only mildly affected the SMC ATPase activity (Figure 5B). We reasoned that ScpA on its own is present as a latent form in terms of stimulating SMC ATPase activity, and that ScpB has an ability to convert ScpA into an active form, probably by changing its conformation.

To test this hypothesis, we sought to introduce artificial disulfide crosslinking to fix the conformation of ScpAB in the closed form, as seen in our crystal structure. In the first pair, ScpA helix H7 (Tyr157) was designed to be crosslinked with the outer surface of $ScpB_{an}$ CTD (Lys144) (Figure 5C, CL1). In the second pair, ScpA strand S2 (Lys168) was designed to be crosslinked with the $ScpB_{an}$ ID region (A94) (Figure 5C, CL2). When the pairs of the polypeptides were coexpressed, purified, and placed under an oxidized condition, designed crosslinking was observed in both cases with high efficiency. As expected from stoichiometry of the complex, half the amount of ScpB was left uncrosslinked in each case, confirming that no unintentional crosslinking occurred under the current condition. We then added the crosslinked molecules of ScpAB in the ATPase assay, and found that the ability of CL1 and CL2 to stimulate SMC ATPase was reduced when crosslinked (Figure 5D, oxi), but was restored to the original level when the crosslinking was reversed (Figure 5D, red).

We next performed a test to see what would happen if ScpA-ScpB interactions were loosened, rather than stabilized, by introducing point mutations (or a short deletion) on either subunit. Introduction of a mutation in the central segment of ScpA (F130R) or deletion of ScpA helix H6 (ΔH6) would disturb the internal ScpAB structure by steric hindrance, thereby preventing the formation of the closed form. As expected, the ScpAB subcomplexes containing these mutations displayed higher levels of ATPase stimulatory activity than did the wild-type ScpAB (Figure 5E). Similarly, when the ScpB ID region, which plays an important role in consolidating the closed form, was mutated (L91R and V92R), the resulting subcomplexes had higher stimulatory activities. Mutant complexes of Y154A in ScpA and A139R in ScpB, which are designed for local disruption of the interface between two ScpB CTDs, displayed a modest ability to stimulate the SMC ATPase. These results further substantiate the idea that our crystal structure of the ScpAB core complex represents a latent form, and that dynamic transformation of the substructure is necessary to stimulate SMC ATPase. We also tested substitution of Met156 of ScpA (Met153 in BsScpA) with arginine to disrupt the interaction of ScpA helix H7 with the $ScpB_{po}$ CTD, and found that the mutant complex exhibited a lower stimulatory activity (Figures 5B and 5E). The subunit stoichiometry of the mutant complex was altered to 1:1 (Figure S7B), which could be explained by aberrant bridging of two ScpA molecules by one ScpB dimer.

Interactions between the SMC Head Domain and ScpAB

To further understand the action of ScpAB, we looked at its physical and functional interactions with the SMC head domain (HD). We coexpressed the three subunits and purified a complex ($HD^{TR}AB$) composed of the HD with the transition-state mutation and ScpAB. In the presence of ATP, $HD^{TR}AB$ dimerized to form a double-sized complex with a stoichiometry of 2:2:4 (Figure 6A, top). However, the formation of this homodimeric species was apparently slow, as a substantial fraction of $HD^{TR}AB$ remained as a monomeric species. On the other hand, when $HD^{TR}AB$ and HD^{TR} were mixed together, they readily formed a heteromeric complex with a stoichiometry of 2:1:2 (Figure 6A, bottom). Thus, $HD^{TR}AB$-$HD^{TR}AB$ engagement is less stable than $HD^{TR}AB$-HD^{TR} engagement, suggesting that the ScpABs on HD^{TR} sterically repel each other, thereby selecting ScpAB-free HD as a preferential engagement partner.

We then performed the ATPase assay using the HD and found that it has a much lower level of basal activity (~2 ATP/min/mol) compared with full-length SMC (Figure 6B). ATP hydrolysis by HDAB was even lower than that by HD. Interestingly, however, when full-length SMC was mixed with a 10-fold excess amount

(D) ATPase activities by full-length SMC (50 nM) in the absence and presence of untreated, oxidized, and reduced forms of CL1 and CL2 (50 nM).
(E) Effects of various point mutations in ScpA and ScpB on the SMC ATPase activity. Details of mutations introduced into each subunit are described in Table S1. A schematic representation of the positions and postulated effects of the point mutations is shown at right (see also Figure S7B for gel filtration profiles of some of the ScpAB mutants).

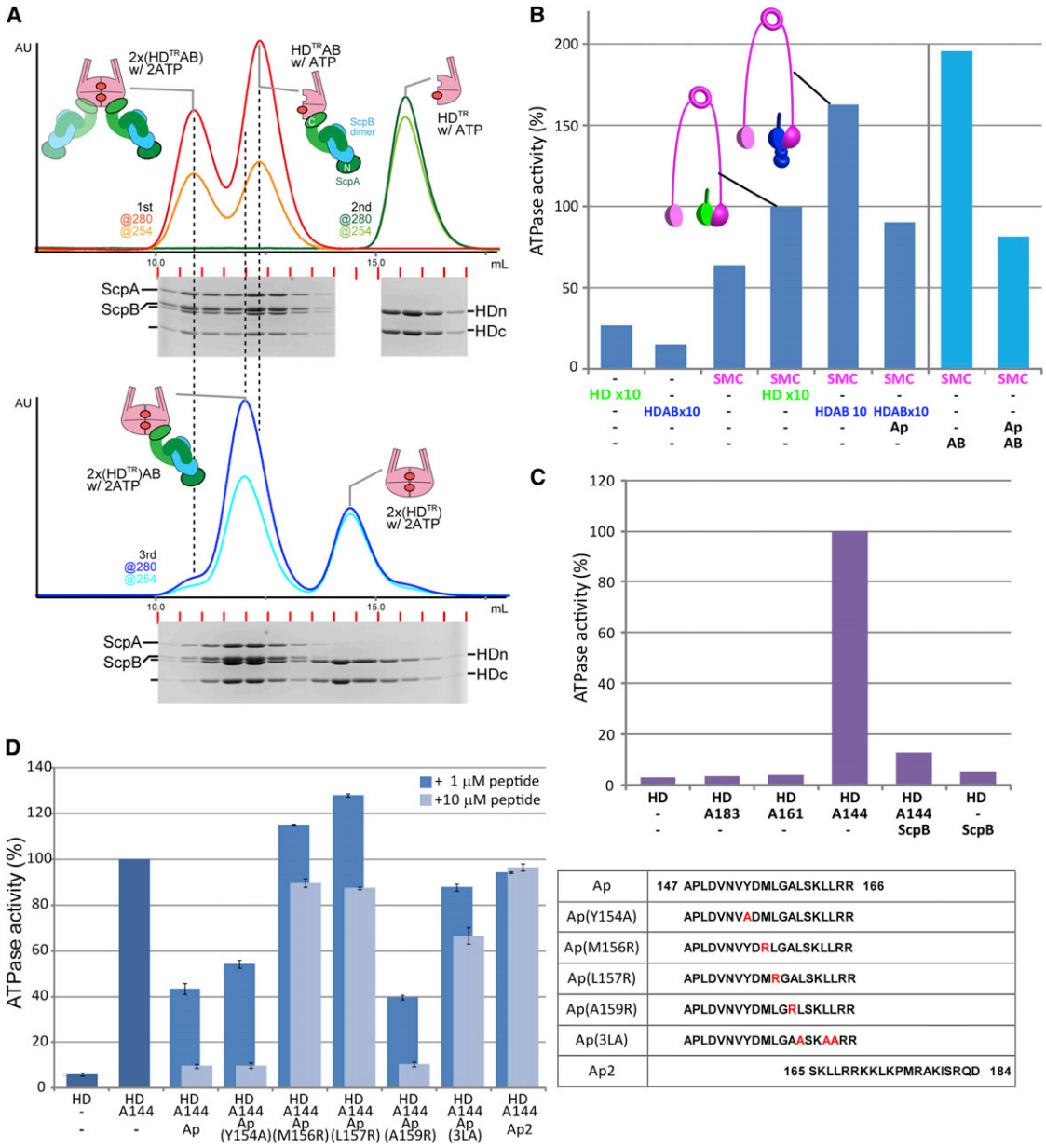

Figure 6. Physical and Functional Interactions between the SMC Head Domain and ScpAB

(A) Molecular species generated by ATP-dependent dimerization of the SMC head domain. (Top) HD^{TR}-ScpAB (red and orange curves) and wild-type HD (green and light green curves) were subjected to separate gel filtration experiments in the presence of ATP, and their elution chromatograms are overlaid. (Bottom) Elution chromatogram of a mixture of HD^{TR}-ScpAB and HD^{TR} (blue and light blue curves) is shown.

(B) ATPase activities of full-length SMC, SMC HD, and their combinations. Different combinations of HD (250 nM), HDAB (250 nM), SMC (25 nM), and ScpAB (50 nM) were used for ATPase assays. Note that 10-fold excess amounts of HD (HD × 10) or HDAB (HDAB × 10) over SMC were used in this set of experiments. In some of the mixtures, the ScpA helix H7 peptide (147–166) was added at a final concentration of 50 μM (indicated by Ap). The activities are plotted as percentages of a reference activity of SMC plus HD × 10.

(C) ATPase activities of HD in the presence of various lengths of ScpA. HD (250 nM) was mixed with the same concentrations of ScpA (183–251) (A183), ScpA (161–251) (A161), or ScpA (144–251) (A144), and ATPase activities of the mixtures were measured. When ScpB was added, a concentration of 500 nM was used. The activities are plotted as percentages of a reference activity of HD plus A144.

(D) ATPase activities of HD plus A144 in the presence of the wild-type or mutated forms of the ScpA helix H7 peptide (147–166) (Ap). HD and A144 (250 nM of each) were mixed with the peptides at a final concentration of 1 μM or 10 μM. The amino acid sequences of the synthetic peptides used here are indicated to the right of the graph. A partially overlapping peptide, Ap2, was used as a negative control. The activities are plotted as percentages of a reference activity of HD plus A144.

See also Figure S7 and Table S1.

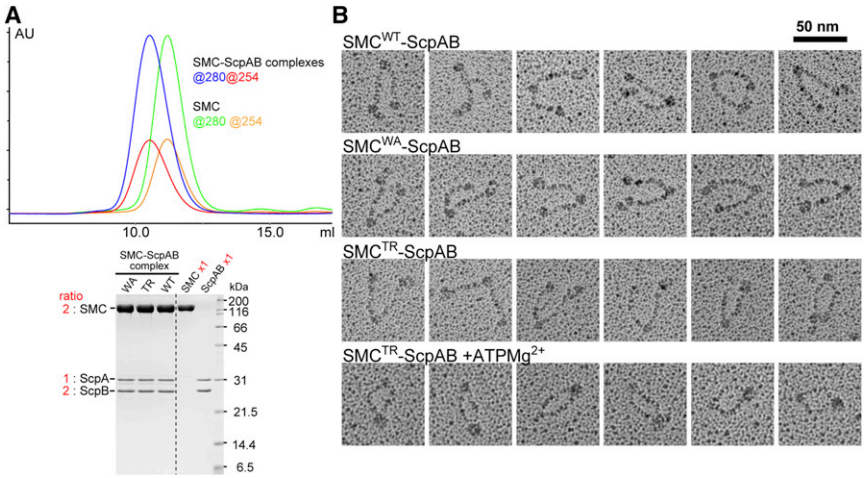

Figure 7. Hydrodynamic Property and Electron Microscopic Analysis of the Full-length SMC-ScpAB Complexes

(A) (Top) SMC-ScpAB (blue and red curves) and SMC dimer (green and orange curves) were subjected to separate gel filtration experiments, and their elution chromatograms are overlaid. (Bottom) The wild-type and mutant (Walker-A [WA] and transition-state [TR]) SMC-ScpAB complexes were subjected to SDS-PAGE and their subunit stoichiometries were estimated using purified SMC and ScpAB as standards.

(B) Electron micrograms of the wild-type (top row) and Walker-A mutant (second row) SMC-ScpAB complexes. The transition-state mutant complexes were visualized in the absence (third row) and presence (fourth row) of ATP-Mg^{2+}.

See also Table S1.

of HD or HDAB, the HDAB stimulated the SMC ATPase activity much more potently than did the HD. This stimulation was reversed when a 20-mer synthetic peptide corresponding to the ScpA helix H7 region (Ap) was added into the reaction mixture. It is therefore most likely that the helix H7 present in HDAB is actively involved in engagement between between HDAB and one HD of the SMC dimer. A similar effect of the peptide was observed when the HDAB was replaced with ScpAB.

We found that addition of ScpA(144–251), which included the helix H7 region and the CTD, greatly stimulated ATP hydrolysis catalyzed by the HD (~9 ATP/min/mol), and that further addition of the ScpB dimer has a negative effect on this stimulatory activity (Figure 6C). Shorter constructs of ScpA (183–251 and 161–251) had little stimulatory activity. These results suggested that the H7 region of ScpA, when not concealed by ScpB, has the ability to stimulate ATP hydrolysis via the HD.

Finally, we asked which residues in the helix H7 region might be important for stimulatory activity. Addition of the wild-type H7 peptide suppressed the ATPase activity of the HD stimulated by ScpA(144–251), whereas three mutant peptides (Ap[M156R], Ap[L157R] and Ap[3LA]) and another overlapping peptide (Ap2) failed to do so (Figure 6D). Thus, not only are the hydrophobic residues in which the mutations were introduced involved in binding to $ScpB_{po}$ CTD, but they are also responsible for controlling the SMC ATPase activity. These findings provide evidence that the helix H7 region facilitates HD-HD engagement through its hydrophobic residues.

Subunit Stoichiometry and Asymmetry of the Full-length SMC-ScpAB Complex

Our crystal structure of the ScpAB core complex revealed that a single ScpA polypeptide chain is uniquely folded by binding to ScpB with 1:2 stoichiometry. To understand the subunit stoichiometry in the context of the SMC-ScpAB holocomplex, full-length SMC, ScpA, and ScpB were coexpressed and purified to homogeneity. The stoichiometry was found to be 2:1:2 as judged by gel filtration and SDS-PAGE (Figure 7A). Introduction of point mutations into the SMC subunit (Walker-A [WA; K37I] or transition-state [TR]) had little effect on the subunit stoichiometry. Electron microscopic observations revealed that the wild-type complex (SMC^{WT}-ScpAB) and the Walker-A mutant complex (SMC^{WA}-ScpAB) predominantly displayed asymmetric V-shaped molecules, in which an extra globular part was attached to one end of the SMC dimer (Figure 7B, first and second rows). It is most likely that the extra part corresponds to the ScpAB complex bound to the SMC head domain. Remarkably, when the transition-state mutant complex (SMC^{TR}-ScpAB), but not SMC^{WT}-ScpAB or SMC^{WA}-ScpAB, was mixed with Mg-ATP, the majority of the molecules displayed a ring-like shape, most likely due to ATP-mediated engagement of the two SMC head domains (Figure 7B, compare the third and fourth rows). The transition-state SMC dimer (SMC^{TR}) also produced similar, ring-shaped molecules in the presence of Mg-ATP, albeit with much lower efficiency compared to SMC^{TR}-ScpAB. These results strongly indicate that although different stoichiometries of the full-length and subcomplexes have been proposed in the literature (Fuentes-Perez et al., 2012; Hirano and Hirano, 2004; Mascarenhas et al., 2005), the ratios determined by the current study are the most likely to be correct. On the other hand, the *E. coli* MukF dimerizes through its N-terminal domains to form a symmetrical structure (along with two MukE dimers) in which the MukF C-terminal domains are available for MukB binding. Coexpression of these three molecules generates heterogeneous species of alternating complexes with the MukB dimer and the MukEF subcomplex (Matoba et al., 2005). On the other hand, a recent fluorescent analysis revealed that a dimer of dimeric MukBEF represents the minimal functional unit in vivo (Badrinarayanan et al., 2012). Thus, the molecular features of MukBEF appear to be intrinsically different from those of the SMC-ScpAB complex.

Functional Link between ScpAB's Dynamic Motion and SMC ATPase Activation

Our current results allow us to describe the relation between dynamic conformational changes of ScpAB and regulation of the SMC ATPase activity (Figure 8). The ScpAB subcomplex binds to the SMC head domain via ScpA's C-terminal domain. Anchoring of the $ScpB_{an}$ CTD to ScpA helix H5 induces proper folding from a free form of ScpA that is inactive in terms of stimulating SMC ATPase. The subsequent binding of the $ScpB_{po}$ CTD and winding motion of the subcomplex physically conceals

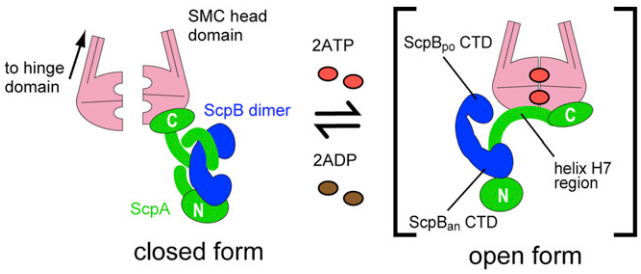

Figure 8. Model for SMC ATPase Activation Coupled with Dynamic Motion of ScpAB

ScpA binds to a head domain of SMC through its C-terminal domain. In the closed form of ScpAB, the ScpB dimer conceals the ScpA helix H7 region. When the SMC head domain engages the other head domain in the presence of ATP, ScpAB may convert to the open form in which the $ScpB_{po}$ CTD is displaced from the helix H7 region. This open form may increase the hydrolysis rate by reposing on the surface of the other SMC head domain.
See also Figure S4.

the helix H7 region of ScpA. Binding of the ScpB dimer ensures proper conversion of ScpA to the latent form that is ready to be activated upon release of the H7 region from weak binding of $ScpB_{po}$ CTD. The observations that ScpAB binds to only one head domain of an SMC dimer (Figures 7A and 7B) strongly suggest that the exposed H7 region would be accommodated by another SMC head domain free of ScpAB. It is reasonable to speculate, however, that this interaction itself is not constitutive and is largely dependent on ATP-mediated engagement of the SMC head domains. Conversely, the availability of the H7 region helps promote or stabilize head-head engagement, thereby stimulating ATP hydrolysis by SMC. Our data are also consistent with the idea that ATP-mediated engagement would facilitate conversion of the ScpAB subcomplex from the closed form to the open form. We suggest that the hydrolysis energy produced upon the engagement is employed to locally unwind the closed form by steric clash between ScpAB and the other SMC head domain.

Recent structural and biochemical data have shown that part of the middle linker region of MukF makes a contact with the other side of engaged MukB HDs and thereby induces dissociation of another MukF from there (Woo et al., 2009). Because this linker region of MukF stimulates ATP hydrolysis via MukB, we speculate that it could play a role equivalent to that of the helix H7 region of ScpA reported in the current study. Although the MukF linker region is disordered in the published structures of MukFE (Gloyd et al., 2011; Woo et al., 2009), we suggest that MukEF could also be converted into a latent form in a way similar to that observed for ScpAB. Our reevaluation of the MukEF structure also implies that the last helix of MukE changes its conformation upon binding to MukF (Figures S4C and S4D) and thereby suppresses the action of the MukF linker region. Thus, despite the differences in the subunit architecture and biochemical properties reported in the literature, it is possible that these particular aspects of ATPase regulation might be shared by the SMC-ScpAB and MukBEF complexes.

In the eukaryotic condensin I complex, the regulatory subcomplex is composed of three large subunits and plays a role in activating SMC ATPase (Kimura and Hirano, 2000). Among these subunits, the CAP-H subunit, a member of the kleisin family, has a central flexible linker flanked by its N- and C-terminal domains. Interestingly, two HEAT repeat-containing subunits (CAP-D2 and CAP-G) have been shown to bind to distinct regions of the central linker of CAP-H (Onn et al., 2007), indicating that H(kleisin)-D2-G has a similar configuration to that of ScpA(kleisin)-$ScpB_2$. It is therefore tempting to speculate that the conformational changes of a kleisin subunit revealed in the current study (i.e., concealment and dynamic release of an activating element from the other regulatory subunits with two different affinity sites) could in fact be conserved in the eukaryotic condensin complexes and participate in controlling the SMC ATPase activity. Future studies should critically address the similarities and differences between the bacterial and eukaryotic complexes to draw an integrated picture of how the SMC protein complexes might work at a mechanistic level.

EXPERIMENTAL PROCEDURES

Crystallization and Data Collection

Crystals of the ScpAB core complex were obtained by sitting-drop vapor diffusion against a reservoir solution containing a mixture of 0.49 M NaH_2PO_4/0.91 M K_2HPO_4 at a narrow pH range of 6.8–7.5 at 20°C. The crystals grew to a typical size of 0.2 × 0.1 × 0.3 mm in the space group $P2_1$, with two oligomeric complexes per asymmetric unit and diffracted to at least 2.6 Å resolution. Derivative crystals for phase determination were prepared by soaking 10 mM CH_3HgCl dissolved in the mother liquor for 1 hr. Crystals of the ScpB NTD dimer complex were produced by hanging-drop vapor diffusion against a reservoir solution containing 100 mM Na malonate-HCl (pH 4.0), 3.0–3.3 M Na formate at 20°C. Orthogonal crystals grew to a typical size of 0.3 × 0.2 × 0.3 mm in the space group *C*2, and diffracted to at least 2.4 Å resolution. Cryoprotection for crystals of both types was achieved by transferring stepwise to the reservoir solution with glycerol to a final concentration of 25% (v/v). All diffraction data were collected at the BL26B2 beamline at SPring-8.

Structure Determination and Refinement

All diffraction data were indexed and integrated with the HKL2000 program and processed further using the CCP4 (Winn et al., 2011) and Phenix program package (Adams et al., 2010). From derivative data of the ScpAB core complex, a total of 12 Hg sites were identified using SHLEX (Sheldrick, 2008), and experimental phases were solved using single anomalous dispersion data measured at the L3 edge of Hg with scattering parameters (f″ = 9.3, Δf = −13.1). High solvent content (~80%) of the complex crystal allowed excellent improvement of the electron density map using RESOLVE (Terwilliger, 2003). For the ScpB NTD dimer complex, coordinates from the ScpAB core complex were used as the search model for molecular replacement with Phaser (Adams et al., 2010), yielding solutions with a good correlation coefficient. After an initial run of AutoBuild (Adams et al., 2010), structural models were built with Coot (Emsley et al., 2010) refined with the CNS (Brunger, 2007) and Phenix program package. Details of the refined models exhibit low *R* factors and good stereochemistry. Drawings of the molecular structures were prepared using Pymol.

Isothermal Titration Calorimetry

Titration experiments were performed at 25°C using iTC_{200} (GE Healthcare). Solutions containing individual domains were dialyzed against and degassed in a buffer containing 50 mM Tris-HCl (pH 7.5) and 100 mM NaCl. The cell was filled with 200 μl of a protein sample and syringe titration was performed by a volume of 0.4 μl for the first-time injection and 1.3 μl for the subsequent 29 injections at an interval of 120 s. Initial concentrations of the samples in the reaction cell and syringe are listed in the legend of Figure 2. Integrated heat data were analyzed using the Origin program according to the manufacturer's instructions. Integrated head data were analyzed using the Origin program according to the manufacturer's instructions, and the parameters ΔH (reaction enthalpy change in cal mol^{-1}), K_b (binding constant in M^{-1}), and n (bound

protein in the cell per protein in the syringe) were estimated. The apparent dissociation constant was calculated as $1/K_b$.

Strains and Plasmids for Molecular Genetics

Routine selection and maintenance of *B. subtilis* strains was performed in Luria Bertani medium at 37°C supplemented, as required, with 5 μg/ml chloramphenicol, 0.5 μg/ml erythromycin, and/or 7 μg/ml neomycin. When necessary, various concentrations of IPTG and xylose were added. Transformation of competent *B. subtilis* cells was performed according to a standard two-step starvation protocol using succinate minimal medium. Strains used in this study are listed in Table S2. Strain BCKA3 was established by transforming the wild-type 168 strain with the plasmid pncAB through single-crossover recombination, resulting in the placement of the full-length *scpAB* genes downstream of the IPTG-inducible *spac* promoter (P*spac*). Similarly, BCKA4 was established with the plasmid pcnB so that only the *scpB* gene came under the control of the P*spac* promoter. DNA fragments encoding various domains of BsScpA and/or BsScpB were subcloned into the plasmid pX. After linearization, the plasmids were used to transform BCKA3 or BCKA4 through double-crossover recombination on *amyE* sequences, so that the domains of BsScpA and/or BsScpB were expressed under the control of the xylose-inducible *xyl* promoter (P*xyl*).

Oxidative Disulfide Crosslinking

Oxidation was carried out using 30 mM Cu(II) phenanthroline complex fleshly prepared by 1:1 mixing with 180 mM phenanthroline in ethanol and 60 mM $CuSO_4$ in water. The stock was diluted to 1:10 with water immediately before use. ScpAB (2–3 μM) dissolved in the GF buffer containing 5% (v/v) glycerol was oxidized by adding 1/10 volume of the copper complex on ice, and the reaction was terminated after 5 min by adding 15 mM EDTA. The mixture was passed through a Superdex 200 10/300 GL column (GE Healthcare) to replace its buffer with the original GF buffer. Reduction of disulfide bonds was performed by treating the mixture with 5 mM DTT at 4°C for 12 hr. Untreated, oxidized, and reduced samples were mixed 1:1 with SDS sample buffer containing 25 mM N-ethylmaleimide and no reducing agent, incubated on ice for 5 min and boiled for 5 min. The products were separated by SDS-PAGE and were stained with Coomassie Brilliant Blue.

ATPase Assay

ATPase activities of the full-length of SMC protein and its head domain were measured using EnzChek Phosphate Assay Kit (Molecular Probes) by quantifying 2-amino-6-mercapto-7-methylpurine riboside (MESG), one of the secondary products of conversion, catalyzed by nucleoside phosphorylase, from MESG and released inorganic phosphate. The reaction was started at 37°C by adding ATP at a final concentration of 0.5 mM into a 200 μl reaction mixture containing 48 mM Tris-HCl (pH 7.5), 110 mM NaCl, 5 mM $MgCl_2$, 0.2 mM dithiothreitol, and 2% glycerol. Absorbance of the secondary reaction product was monitored at 360 nm on a microplate reader, SH-9000 (Corona).

Gel Filtration

The dimerized head domain was monitored by gel filtration chromatography (Superdex 200 10/300 GL) in a running buffer containing 20 mM HEPES-HCl (pH 7.5), 150 mM NaCl, 1 mM $MgCl_2$, and 0.1 mM ATP at 4°C. Loaded protein samples were mixed in the running buffer with extra additives of 10 mM $MgCl_2$ and 1 mM ATP at room temperature. Wild-type and mutant complexes composed of full-length SMC and ScpAB were subjected to a gel filtration column (Superose 6 10/300 GL) in a running buffer containing 20 mM Tris-HCl (pH 7.5) and 300 mM NaCl at 4°C. Subunit stoichiometry of the purified complexes was estimated by comparison with individually purified standard samples (SMC and ScpAB complex) on SDS-PAGE using LAS3000 (Fuji film).

Electron Microscopy

Purified SMC-ScpAB complexes were diluted with 50% (v/v) glycerol containing 0.3 M ammonium acetate to a final concentration of ~0.03 mg/ml. When necessary, the buffer was supplemented with 3 mM $MgCl_2$ and ATP. The samples were sprayed onto a freshly cleaved mica surface and dried under vacuum. The complex molecules were rotary-shadowed with platinum at an angle of 6° and supported with carbon at an angle of 90° (HITACHI HUS-5GB). The shadowed platinum films were removed from the mica on the water surface and mounted on copper grids. The replicas were examined at 40,000-fold magnification using an electron microscope (JEOL JEM-1230) operating at 80 kV.

ACCESSION NUMBERS

The Protein Data Bank coordinates for the crystal structure of the *Geobacillus stearothermophilus* ScpAB complex and the ScpB NTD dimer complexed with ScpA peptide have been deposited under the ID codes 3W6J and 3W6K, respectively.

SUPPLEMENTAL INFORMATION

Supplemental Information includes seven figures, two tables, and Supplemental Experimental Procedures and can be found with this article online at http://dx.doi.org/10.1016/j.str.2013.02.016.

ACKNOWLEDGMENTS

We are grateful to Drs. T. Hikima and G. Ueno operating BL26B beamlines at SPring-8 for assistance with data collection. We are indebted to Drs. M. Usui and K. Otsuki for analyses by mass spectrometry; T. Kikitsu, Y. Tahara, and H. Yamamoto for analyses by electron microscopy; and Drs. Y. Takeda and T. Kobayashi for kindly permitting us to use a calorimeter. We also thank Drs. D. Jeruzalmi, F. Kawamura, K. Kobayashi, and S. Kosono for providing materials and technical advice. This work was supported by Grants-in-Aid for Science Research to K.K. and a Grant-in-Aid for Specially Promoted Research to T.H. from the Ministry of Education, Culture, Sports, Science, and Technology of Japan.

Received: January 4, 2013
Revised: February 14, 2013
Accepted: February 17, 2013
Published: March 28, 2013

REFERENCES

Adams, P.D., Afonine, P.V., Bunkóczi, G., Chen, V.B., Davis, I.W., Echols, N., Headd, J.J., Hung, L.W., Kapral, G.J., Grosse-Kunstleve, R.W., et al. (2010). PHENIX: a comprehensive Python-based system for macromolecular structure solution. Acta Crystallogr. D Biol. Crystallogr. *66*, 213–221.

Anderson, D.E., Losada, A., Erickson, H.P., and Hirano, T. (2002). Condensin and cohesin display different arm conformations with characteristic hinge angles. J. Cell Biol. *156*, 419–424.

Badrinarayanan, A., Reyes-Lamothe, R., Uphoff, S., Leake, M.C., and Sherratt, D.J. (2012). In vivo architecture and action of bacterial structural maintenance of chromosome proteins. Science *338*, 528–531.

Britton, R.A., Lin, D.C., and Grossman, A.D. (1998). Characterization of a prokaryotic SMC protein involved in chromosome partitioning. Genes Dev. *12*, 1254–1259.

Brunger, A.T. (2007). Version 1.2 of the Crystallography and NMR system. Nat. Protoc. *2*, 2728–2733.

Cui, Y., Petrushenko, Z.M., and Rybenkov, V.V. (2008). MukB acts as a macromolecular clamp in DNA condensation. Nat. Struct. Mol. Biol. *15*, 411–418.

Emsley, P., Lohkamp, B., Scott, W.G., and Cowtan, K. (2010). Features and development of Coot. Acta Crystallogr. D Biol. Crystallogr. *66*, 486–501.

Fennell-Fezzie, R., Gradia, S.D., Akey, D., and Berger, J.M. (2005). The MukF subunit of *Escherichia coli* condensin: architecture and functional relationship to kleisins. EMBO J. *24*, 1921–1930.

Fuentes-Perez, M.E., Gwynn, E.J., Dillingham, M.S., and Moreno-Herrero, F. (2012). Using DNA as a fiducial marker to study SMC complex interactions with the atomic force microscope. Biophys. J. *102*, 839–848.

Gloyd, M., Ghirlando, R., and Guarné, A. (2011). The role of MukE in assembling a functional MukBEF complex. J. Mol. Biol. *412*, 578–590.

Graumann, P.L., and Knust, T. (2009). Dynamics of the bacterial SMC complex and SMC-like proteins involved in DNA repair. Chromosome Res. *17*, 265–275.

Haering, C.H., Schoffnegger, D., Nishino, T., Helmhart, W., Nasmyth, K., and Löwe, J. (2004). Structure and stability of cohesin's Smc1-kleisin interaction. Mol. Cell *15*, 951–964.

Hirano, T. (2012). Condensins: universal organizers of chromosomes with diverse functions. Genes Dev. *26*, 1659–1678.

Hirano, M., and Hirano, T. (2004). Positive and negative regulation of SMC-DNA interactions by ATP and accessory proteins. EMBO J. *23*, 2664–2673.

Holm, L., and Rosenström, P. (2010). Dali server: conservation mapping in 3D. Nucleic Acids Res. *38*(Web Server issue), W545–W459.

Jensen, R.B., and Shapiro, L. (1999). The *Caulobacter crescentus smc* gene is required for cell cycle progression and chromosome segregation. Proc. Natl. Acad. Sci. USA *96*, 10661–10666.

Kim, J.S., Shin, D.H., Pufan, R., Huang, C., Yokota, H., Kim, R., and Kim, S.H. (2006). Crystal structure of ScpB from *Chlorobium tepidum*, a protein involved in chromosome partitioning. Proteins *62*, 322–328.

Kim, J.S., Lee, S., Kang, B.S., Kim, M.H., Lee, H.S., and Kim, K.J. (2008). Crystal structure and domain characterization of ScpB from *Mycobacterium tuberculosis*. Proteins *71*, 1553–1556.

Kimura, K., and Hirano, T. (2000). Dual roles of the 11S regulatory subcomplex in condensin functions. Proc. Natl. Acad. Sci. USA *97*, 11972–11977.

Lindow, J.C., Kuwano, M., Moriya, S., and Grossman, A.D. (2002). Subcellular localization of the *Bacillus subtilis* structural maintenance of chromosomes (SMC) protein. Mol. Microbiol. *46*, 997–1009.

Losada, A., and Hirano, T. (2005). Dynamic molecular linkers of the genome: the first decade of SMC proteins. Genes Dev. *19*, 1269–1287.

Mascarenhas, J., Soppa, J., Strunnikov, A.V., and Graumann, P.L. (2002). Cell cycle-dependent localization of two novel prokaryotic chromosome segregation and condensation proteins in *Bacillus subtilis* that interact with SMC protein. EMBO J. *21*, 3108–3118.

Mascarenhas, J., Volkov, A.V., Rinn, C., Schiener, J., Guckenberger, R., and Graumann, P.L. (2005). Dynamic assembly, localization and proteolysis of the *Bacillus subtilis* SMC complex. BMC Cell Biol. *6*, 28.

Matoba, K., Yamazoe, M., Mayanagi, K., Morikawa, K., and Hiraga, S. (2005). Comparison of MukB homodimer versus MukBEF complex molecular architectures by electron microscopy reveals a higher-order multimerization. Biochem. Biophys. Res. Commun. *333*, 694–702.

Melby, T.E., Ciampaglio, C.N., Briscoe, G., and Erickson, H.P. (1998). The symmetrical structure of structural maintenance of chromosomes (SMC) and MukB proteins: long, antiparallel coiled coils, folded at a flexible hinge. J. Cell Biol. *142*, 1595–1604.

Moriya, S., Tsujikawa, E., Hassan, A.K., Asai, K., Kodama, T., and Ogasawara, N. (1998). A *Bacillus subtilis* gene-encoding protein homologous to eukaryotic SMC motor protein is necessary for chromosome partition. Mol. Microbiol. *29*, 179–187.

Nasmyth, K., and Haering, C.H. (2005). The structure and function of SMC and kleisin complexes. Annu. Rev. Biochem. *74*, 595–648.

Onn, I., Aono, N., Hirano, M., and Hirano, T. (2007). Reconstitution and subunit geometry of human condensin complexes. EMBO J. *26*, 1024–1034.

Onn, I., Heidinger-Pauli, J.M., Guacci, V., Unal, E., and Koshland, D.E. (2008). Sister chromatid cohesion: a simple concept with a complex reality. Annu. Rev. Cell Dev. Biol. *24*, 105–129.

Peters, J.M., Tedeschi, A., and Schmitz, J. (2008). The cohesin complex and its roles in chromosome biology. Genes Dev. *22*, 3089–3114.

Petrushenko, Z.M., Lai, C.H., and Rybenkov, V.V. (2006). Antagonistic interactions of kleisins and DNA with bacterial Condensin MukB. J. Biol. Chem. *281*, 34208–34217.

Sheldrick, G.M. (2008). A short history of SHELX. Acta Crystallogr. A *64*, 112–122.

Soppa, J., Kobayashi, K., Noirot-Gros, M.F., Oesterhelt, D., Ehrlich, S.D., Dervyn, E., Ogasawara, N., and Moriya, S. (2002). Discovery of two novel families of proteins that are proposed to interact with prokaryotic SMC proteins, and characterization of the *Bacillus subtilis* family members ScpA and ScpB. Mol. Microbiol. *45*, 59–71.

Terwilliger, T.C. (2003). SOLVE and RESOLVE: automated structure solution and density modification. Methods Enzymol. *374*, 22–37.

Volkov, A., Mascarenhas, J., Andrei-Selmer, C., Ulrich, H.D., and Graumann, P.L. (2003). A prokaryotic condensin/cohesin-like complex can actively compact chromosomes from a single position on the nucleoid and binds to DNA as a ring-like structure. Mol. Cell. Biol. *23*, 5638–5650.

Winn, M.D., Ballard, C.C., Cowtan, K.D., Dodson, E.J., Emsley, P., Evans, P.R., Keegan, R.M., Krissinel, E.B., Leslie, A.G., McCoy, A., et al. (2011). Overview of the CCP4 suite and current developments. Acta Crystallogr. D Biol. Crystallogr. *67*, 235–242.

Woo, J.S., Lim, J.H., Shin, H.C., Suh, M.K., Ku, B., Lee, K.H., Joo, K., Robinson, H., Lee, J., Park, S.Y., et al. (2009). Structural studies of a bacterial condensin complex reveal ATP-dependent disruption of intersubunit interactions. Cell *136*, 85–96.

Yamazoe, M., Onogi, T., Sunako, Y., Niki, H., Yamanaka, K., Ichimura, T., and Hiraga, S. (1999). Complex formation of MukB, MukE and MukF proteins involved in chromosome partitioning in *Escherichia coli*. EMBO J. *18*, 5873–5884.

